Power Maximization and Fatigue-Load Mitigation in a Wind-turbine Array by Active Yaw Control: an LES Study

Power Maximization and Fatigue-Load Mitigation in a Wind-turbine Array by Active Yaw Control: an LES Study

Mou Lin, Fernando Porté-Agel

Wind Engineering and Renewable Energy Laboratory (WIRE), École Polytechnique Fédérale de Lausanne (EPFL), EPFL-ENAC-IIE-WIRE, CH-1015 Lausanne, Switzerland

E-mail: mou.lin@epfl.ch, fernando.porte-agel@epfl.ch

Abstract. In this study, we perform a multi-objective parametric study for an array of three miniature wind turbines subjected to active yaw control (AYC), with the objectives of maximizing the power and minimizing the fatigue loads. Using the time series extracted from large-eddy simulation (LES), we compute the mean power and the yaw-moment damage equivalent load (DEL) at every point of a finite decision space spanned by the yaw angles of the first two turbines. The mean power outputs simulated with LES are compared with those measured in the wind tunnel, and a good agreement is found between the two. The Pareto front of different yaw configurations is extracted in the objective space of AYC and the Pareto-optimal strategies are identified in the decision space. We find that most of the Pareto-optimal strategies share the characteristic of moderately decremental yaw angles. We also find that the strategies with a small yaw angle for the first wind turbine are inefficient since they incur significant increases in fatigue while only achieving marginal power gains. The results indicate that the decision space of algorithms searching for optimal AYC strategies can be significantly reduced a priori with the consideration of load mitigation in the optimization.

1. Introduction

Amid the rapid growth of the global wind-power capacity, maximizing the efficiency of wind farms has become a critical issue for wind energy researchers and developers. One of the most important problems encountered in wind farms within restricted areas is the interference of upwind wind-turbine wakes with downwind turbines [1, 2]. This phenomenon induces a significant power loss and an increase in fatigue loads in wind farms [3–5]. Various measures have been proposed by researchers to curb these adverse effects [6–8], including active yaw control (AYC), which has recently drawn rising interest in the wind energy research community [9–11]. In AYC, some wind turbines are intentionally misaligned with the incoming wind direction to steer their wakes away from downstream turbines, achieving a net power gain in the entire wind farm.

To validate the effectiveness of AYC strategy, several computational and experimental studies have been carried out so far. Gebraad et al. [12] used a reduced-order solver to optimize the energy production of a hypothetical wind farm subjected to AYC. The same optimization framework was further applied to a real wind farm by Gebraad et al. [13]. Validated with a large-eddy simulation (LES), they indicated that AYC can increase the annual energy production of

the wind farm by 5%. Archer and Vasel-Be-Hagh [14] used LES to study the effect of applying AYC at different rows in a wind-turbine array. They found that, in terms of net power gain, applying AYC at the front rows and deep rows in a turbine array is more favourable than applying it at the mid rows. Bastankhah and Porté-Agel [11] measured the power outputs of different yaw strategies for an array of five wind turbines in wind-tunnel experiments. The optimal strategy they found is a configuration of gradually decreasing yaw angles from upstream to downstream turbines. Under typical inflow conditions, they reported that such an optimal yaw strategy could yield an 18% power gain from the baseline case. Besides static yaw control, Munters et. al. [15] indicated the potential of applying dynamic yaw strategies in wind farms by changing the yaw angles transiently. The dynamic strategies were sought by an LES-based adjoint-optimization framework.

Besides power optimization, the structural impacts of applying AYC have also been examined by researchers. While many previous studies have suggested that AYC can alleviate the fatigue loads applied on wind turbines in some circumstances [16], some researchers have also indicated possible adverse structural effects for wind turbines under constant yaw conditions [17]. Van Dijk et al. [18] carried out a joint optimization of power maximization and load mitigation for a three-turbine array. In their study, the fatigue loads were quantified as the differences of the bending moments the blades endure when they sweep through the partially overlapped wakes computed by a steady-state solver, and the effect of wake turbulence was not considered in the evaluation of fatigue. A wind tunnel study was also performed by Bartl et al. [19] to investigate the increase of the yaw moment acting on wind turbines under AYC. They found that, while in the case of full wake overlapping the net power gain is achieved at the cost of increasing the yaw moment, in the case of partial wake overlapping AYC can increase the power output and mitigate the yaw moment at the same time.

As the literature shows, when applying AYC to optimize the power output in wind farms, it is essential to also take the fatigue loads into account to avoid the potential adverse structural impact offsetting the benefit of power gains. Therefore, it is of great importance to understand the characteristics of the Pareto-optimal strategies, i.e., the strategies that achieve the largest power output at a given level of fatigue loads and endure the lowest fatigue loads at a given power output, in the decision space of AYC.

To address this issue, in this study we use LES to investigate the distribution the Pareto-optimal strategies for a minimal non-trivial case in AYC: a three-turbine array with two controlled turbines. The main advantage of using LES is that the transient non-uniform aerodynamic forces acting on the rotor disk can be directly extracted from the simulation to evaluate the fatigue loads of wind turbines in turbulent incoming flows. In this configuration, the first two upwind turbines are subjected to AYC in a finite discrete decision space $\mathbf{\Gamma} = \{\gamma_1 : 0^\circ, ..., 31^\circ\} \times \{\gamma_2 : 0^\circ, ..., 31^\circ\}$ and the last wind turbine is fixed to 0° yaw angle. The objective space $\mathbf{\Omega}$ is spanned by the mean total power of the wind-turbine array P_{tot} and the total damage equivalent load (DEL) induced by the transient yaw moment acting on the turbines. The choice of the yaw moment as the representative metric among other loads acting on the turbine is due to the frequency of the mechanical failure modes shown in the operational data [20].

The rest of the paper is structured as follows. First, in Section 2, the numerical configurations used in the simulations and the methodology for evaluating the power and the fatigue loads are presented. In Section 3, the power outputs of four typical yaw strategies are analyzed and compared with wind-tunnel measurements. Then, the results of the mean total power and the DEL are calculated at every point of the decision space $\mathbf{\Gamma}$. The Pareto front is extracted in the objective space $\mathbf{\Omega}$ and the corresponding Pareto-optimal strategies are identified in the decision space $\mathbf{\Gamma}$. Finally, in Section 4, conclusions are drawn from the results and followed by a discussion of possible future researches.

2. Methodology

2.1. Governing equations

In this study, we use the WiRE-LES code developed at the Laboratory of Wind Engineering and Renewable Energy (WIRE) of the École Polytechnique Fédérale de Lausanne (EPFL), which solves the spatially-filtered incompressible Navier-Stokes equations:

$$\begin{aligned} \frac{\partial \widetilde{u}_i}{\partial x_i} &= 0, \\ \frac{\partial \widetilde{u}_i}{\partial t} + \widetilde{u}_j \left(\frac{\partial \widetilde{u}_i}{\partial x_j} - \frac{\partial \widetilde{u}_j}{\partial x_i} \right) &= -\frac{\partial \widetilde{p}^*}{\partial x_i} - \frac{\partial \tau_{ij}}{\partial x_j} - \frac{f_i}{\rho} + \frac{F_p}{\rho}\delta_{i1}, \end{aligned} \tag{1}$$

where $\widetilde{u}_i$ is the spatially filtered velocity component in the i-direction ($i = 1, 2, 3$), $\widetilde{p}^*$ is the modified kinematic pressure, f_i is the body force exerted by the wind turbine on the flow, F_p is the pressure gradient imposed to the flow, and $\tau_{ij} = \widetilde{u_i u_j} - \widetilde{u}_i \widetilde{u}_j$ is the kinematic sub-grid scale (SGS) stress.

2.2. Numerical setup

WiRE-LES solves the filtered governing equations numerically with the pseudo-spectral method in the horizontal directions and a second-order finite difference scheme in the vertical direction. The Adam-Bashforth method is used for the integration over time. The sub-grid scale (SGS) stress term is parametrized using the scale-dependent dynamic model [21] with Lagrangian averaging [22]. The body-force term for wind-turbine forces is parametrized by the rotational actuator disk model [23–25].

The simulation domain (7.68 m×0.96 m×0.48 m) is uniformly discretized into $192 \times 96 \times 48$ grid cells. A wind-turbine array with three WiRE-01 miniature wind turbines [26] is placed along the center-line of the simulation domain (Figure 1). The physical simulation time is 25 seconds and the first five seconds are excluded in the statistical analysis. The boundary conditions of the simulation domain are summarized in Table 1.

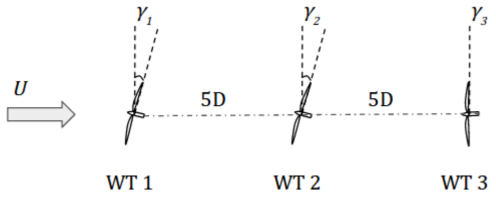

Figure 1: Schematic plot (top view) of the wind-turbine array.

Table 1: Summary of boundary conditions.

Boundary	Description
Inlet/outlet	Periodic boundary with precursor inflow.
Lateral	Periodic boundary.
Top	Non-penetration friction-less wall.
Bottom	Non-penetration wall with a specified wall-shear stress [21, 25].

A turbulent inflow is enforced at the inlet, which is generated by a precursor simulation of a fully-developed pressure-driven neutral boundary-layer flow. The main characteristic quantities of the precursor inflow are summarized in Table 2. Those quantities are consistent with their counterparts in the wind-tunnel experiments performed by [11].

Table 2: Main characteristics of the incoming boundary-layer flow.

Inflow characteristic	**Value**
Boundary-layer height (H)	0.48 m
Hub-height incoming velocity ($\overline{u}_h$)	4.8 m/s
Hub-height turbulence intensity (I_u)	7%
Surface roughness length (z_o)	0.01 mm
Friction velocity (u_*)	0.2 m/s

2.3. Power and load evaluation

As the rotational actuator disk model for wind turbines directly resolves the forces acting on the rotor disk, we can obtain the time series of the mechanical power P and the yaw moment M_z of a given wind turbine from the simulation as follows:

$$\begin{aligned} P &= \omega \sum_{j=1}^{N_{be}} r_{o,j} F_{\theta j}, \\ M_z &= \sum_{j=1}^{N_{be}} r_{z,j} F_{xj}, \end{aligned} \tag{2}$$

where ω is the rotor angular velocity; $r_{o,j}$ and $r_{z,j}$ are the distances of the jth blade element to the hub center o and to the vertical center-line of the rotor disk, respectively; $F_{\theta j}$ and F_{xj} are the rotor-tangential force and the rotor-normal force acting on the jth blade element, respectively; N_{be} is the total number of blade elements.

After obtaining the yaw-moment time series, we apply the rainflow cycle-counting algorithm, the Palgrem Miner's rule and the Goodman diagram to compute the DEL induced by the yaw moment in the turbine array [27–29]:

$$M_{DEL} = \left(\frac{\sum_{i=1}^{n_b} n_i M_i^m}{N_{ref}} \right)^{1/m}, \tag{3}$$

where n_b is the bin number of the rainflow cycle-counting; n_i and M_i are the cycle count and the corrected cycle range of the ith bin and N_{ref} is the reference cycle number; m is a material-specific parameter and is set as 4. The cycle range M_i is corrected by the Goodman's rule to take the effect of the mean load on fatigue into account:

$$M_i = \frac{M_{i,ori}}{1 - \frac{M_m}{\sigma M_{max}}}, \tag{4}$$

where $M_{i,ori}$ is the original cycle range extracted from the time series; M_m is the mean load and M_{max} is the maximum yaw moment in the time series; σ is a parameter for determining the ultimate load $M_u = \sigma M_{max}$ and is chosen as 1.5.

The mean total power and the total yaw-moment DEL of the wind-turbine array form the objective space $\mathbf{\Omega}$ in this study. To maximize the power output and minimize the DEL in the turbine array, we can extract the Pareto front in the objective space $\mathbf{\Omega}$ and study the distribution of the Pareto-optimal strategies in the decision space.

3. Results

3.1. Inflow condition

Figure 2 shows the comparison of the vertical profiles of the normalized mean streamwise wind speed and streamwise turbulence intensity obtained from the precursor LES and the wind-tunnel measurements [11], respectively. A good agreement between the two is observed, particularly at turbine level.

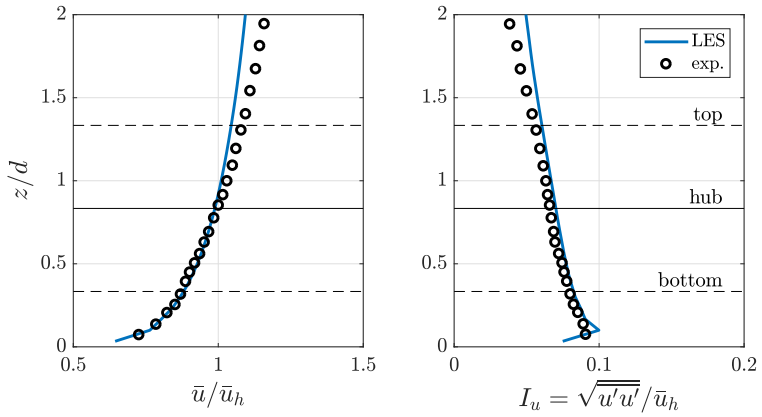

Figure 2: Vertical profiles of the normalized mean streamwise velocity component $\overline{u}/\overline{u}_h$ and the streamwise turbulence intensity I_u. Blue solid lines represent the LES results and black circles represent the measurements.

3.2. Velocity deficit

Figure 3 shows the top-view contours of the normalized mean streamwise velocity deficit $\Delta\overline{u}/\overline{u}_{hub}$ in the horizontal plane at the hub height. Two representative cases are chosen from the decision space $\mathbf{\Gamma}$: the baseline case without yaw $(0°, 0°, 0°)$ and the yawing case $(30°, 30°, 0°)$. As shown in Figure 3, the wakes behind the yawed turbines are deflected from the center-line of the wind-turbine array. The wake deflection leads to a stronger wake for the last non-yawed turbine. The phenomenon of secondary wake steering [30–32] can also be observed in Figure 3: The wakes of downstream turbines experience additional wake deflection due to the fact that they face the incoming wake of a yawed upstream turbine, which has non-zero lateral velocity. This is also the reason why the wake of the last turbine is deflected, even if the turbine is not yawed.

3.3. Power output

To validate the LES results, we compare the power outputs obtained from LES and the wind-tunnel measurements performed by Bastankhah and Porté-Agel [11] for four cases representing four typical scenarios:

- the baseline case without yaw $(0°, 0°, 0°)$;
- the case in which the first two turbines are yawed with the same angle $(30°, 30°, 0°)$;
- the case in which only the first turbine is yawed $(20°, 0°, 0°)$;

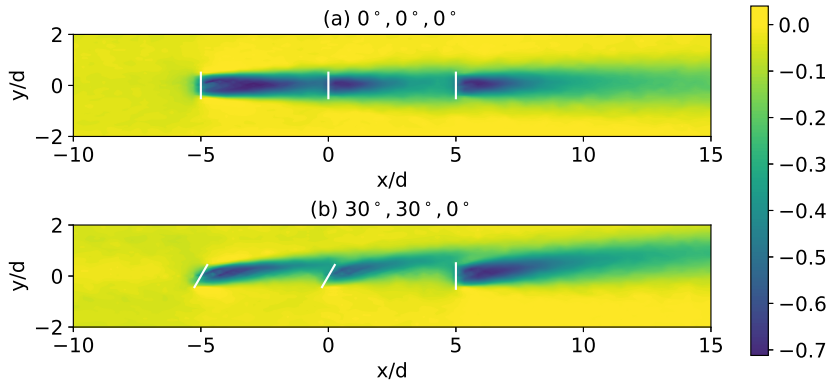

Figure 3: Top-view contours of the normalized streamwise mean velocity deficit $\Delta\overline{u}/\overline{u}_h$ in the horizontal plane at the hub height obtained from the LES results. White lines outline the miniature wind turbines.

- the case in which the first two turbines are yawed with moderately decremental yaw angles $(25°, 20°, 0°)$.

As shown in Figure 4, for all four cases, the total power outputs P_{tot} extracted from the LES results are in good agreement with the wind-tunnel measurements. The largest power output is found in case $(25°, 20°, 0°)$ for LES and the wind-tunnel measurements. The largest relative error (3.8 %) of the total power prediction is also observed in case $(25°, 20°, 0°)$ where the power outputs from LES for each turbine are all slightly underestimated. It is worth noting that the better total-power predictions obtained by other cases are partially due to the cancellation of errors among each turbine. When considering the maximum error of the power for each turbine, we find that the cases that encounter stronger wake superposition, i.e., $(0°, 0°, 0°)$ and $(20°, 0°, 0°)$, are less consistent with the wind-tunnel measurements than the cases which have larger wake deflections, i.e., $(30°, 30°, 0°)$ and $(25°, 20°, 0°)$. The improvements to the baseline and the relative errors of the LES results to the wind tunnel measurements are summarized in Table 3.

Table 3: Summary of the improvements to the baseline case and the errors to the experiments in LES cases.

LES case	Improvements	Errors comparing to the experiments
$0°, 0°, 0°$	baseline	-2.0%
$20°, 0°, 0°$	+2.8%	-1.46%
$30°, 30°, 0°$	+5.9%	-0.04%
$25°, 20°, 0°$	+6.0%	-3.8%

3.4. Yaw moment load

As we have discussed previously, the impact of the transient aerodynamic loads acting on wind turbines is another important factor to be considered when applying AYC. Figure 5 shows the

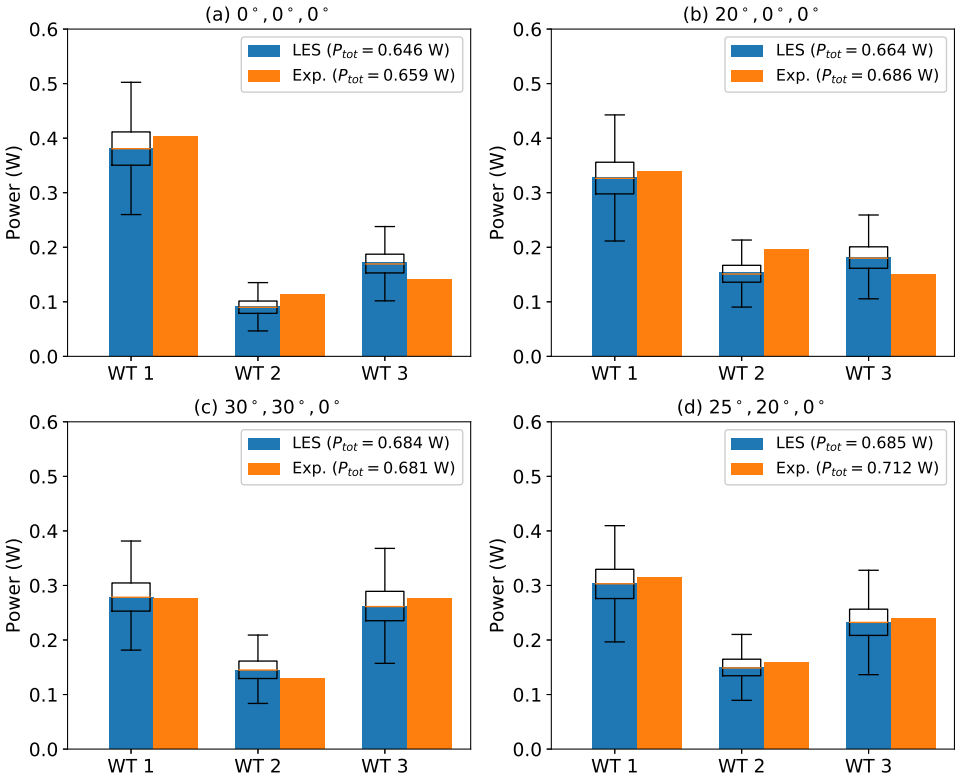

Figure 4: Comparisons of power outputs extracted from LES and the wind-tunnel measurements for four typical yaw scenarios. The maximum/minimum values and the range between the first quartile and the third quartile of the time series of the power extracted from LES are shown in the box plot.

time series of the yaw moment that the last wind turbine in the array (WT 3) endures in the baseline case $(0°, 0°, 0°)$ and the yawing case $(30°, 30°, 0°)$. Although WT 3 is kept non-yawed for both cases, due to the secondary wake steering effect, the characteristics of the yaw moment of WT 3 in the yawing case $(30°, 30°, 0°)$ are still significantly different from the baseline case. Using the rainflow counting algorithm, we extract the load cycles from the time series and study their statistical distributions (Figure 6). After AYC is applied to the upstream turbines, the mean of the load cycle average (defined as $(M_{i,max} + M_{i,min})/2$ for each cycle) is increased while the variance is decreased. The distribution of the load cycle range (defined as $M_{i,max} - M_{i,min}$ for ith cycle) in the yawing case $(30°, 30°, 0°)$ has a thinner tail than its counterpart in the baseline case. Assuming an exponential distribution of the load cycle range, one can see that this difference also indicates that the yawing case has a smaller statistical variance for the cycle range than the baseline case.

3.5. Pareto-optimal strategy in decision space

From the previous discussion, one can see that applying AYC not only changes the power output of the wind-turbine array but also significantly alters the statistical properties of the aerodynamic loads. To quantify the impact of different cycling loads acting on the turbines, we adopt the DEL, a widely used metric in fatigue analysis. Figure 7 shows the total mean power increase and the total DEL increase with respect to the baseline case at each point in the discrete decision space $\mathbf{\Gamma}$. We find that both quantities reach their maximum at the same point $(31°, 20°)$, although the relative increase of DEL is much larger than the power.

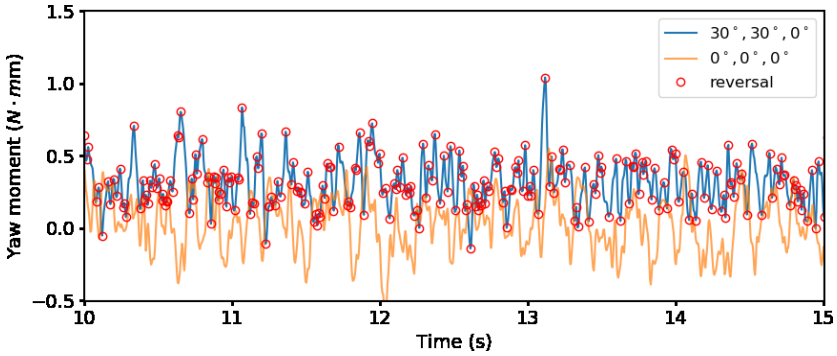

Figure 5: Time-series segments (from 10 s to 15 s) of the yaw moments acting on the last wind turbine in the array. Red circles mark the reversal points extracted for the rainflow load-cycle counting.

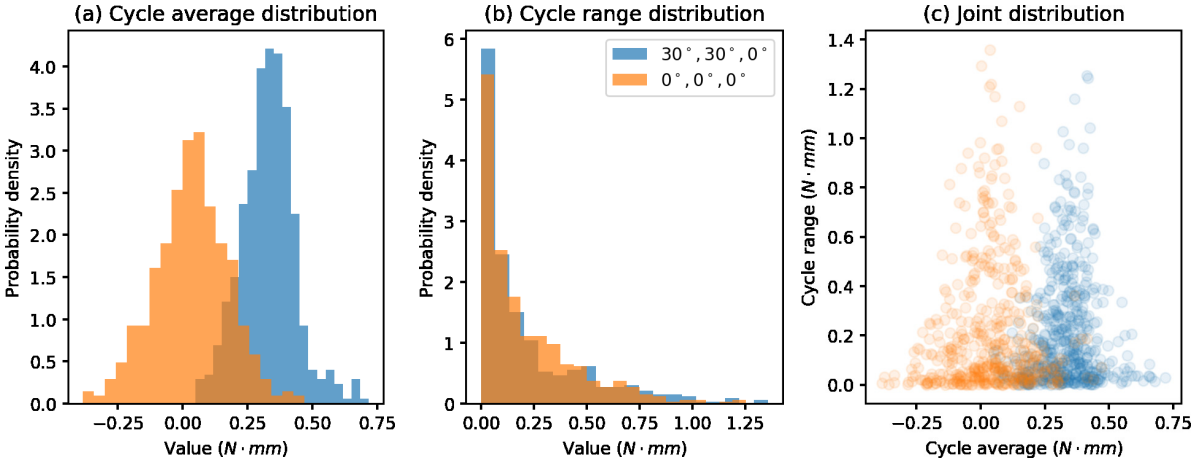

Figure 6: Statistical distributions of the average and the range of the yaw-moment load cycle encountered by the last non-yawed turbine.

Figure 8(a) shows the decision points in the objective space $\mathbf{\Omega}$ spanned by the increase of DEL and power gain. With the goal of power maximization and DEL minimization, Pareto-optimal strategies (red dots) are also extracted in the objective space $\mathbf{\Omega}$. The Pareto-optimal decision points are then transformed back to the decision space $\mathbf{\Gamma}$ (Figure 8(b)). A heat-map is also constructed using a Gaussian kernel to highlight the distribution of Pareto points in $\mathbf{\Gamma}$.

From Figure 8(a), we observe that the decision points are concentrated in a narrow band, extending from the lower-left corner to the upper-right corner of the decision space $\mathbf{\Omega}$. Such a pattern indicates that the room for the ideal Pareto improvement, i.e., reducing DEL (moving left) while increasing power (moving up), is largely limited in this array where the location of the three turbines are aligned with the incoming wind. Comparing within the Pareto-optimal strategies, we find that the Pareto front resembles a curve with smaller slopes in the region where DEL increases less than 20%, and a constant slope ($k \approx 0.25$) as DEL becomes larger. From Figure 8(b), we find that the Pareto-optimal strategies identified in the objective space are clustered in a region in the decision space corresponding to the moderately decremental yaw strategies ($\gamma_1 - \gamma_2 < 20°$). 93% of Pareto-optimal strategies are not situated in the region representing the incremental yaw strategies ($\gamma_1 < \gamma_2$), the strategies where only the first turbine

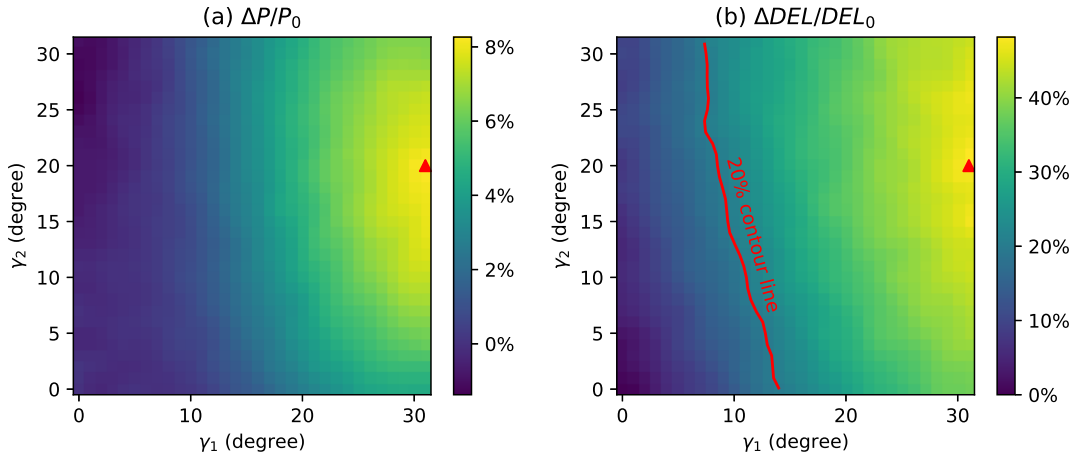

Figure 7: Contours of the relative increase of power (a) and DEL (b) in the decision space $\mathbf{\Gamma}$. Red triangles represent the maximum location $(31°, 20°)$ for both quantities.

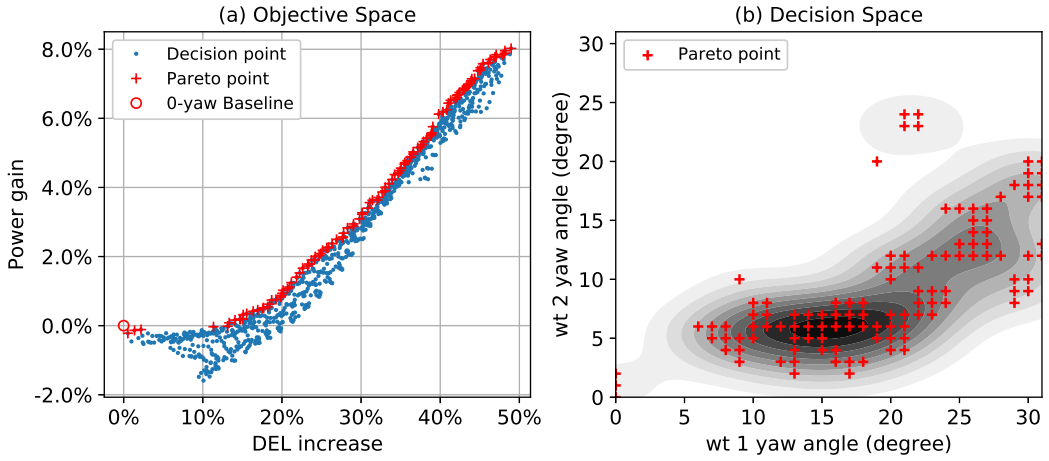

Figure 8: (a) Pareto front identified in the objective space $\mathbf{\Omega}$. (b) The distribution of Pareto points in the decision space $\mathbf{\Gamma}$ (Overlapped with a heatmap contour). Red dots represent the Pareto-optimal strategies.

is yawed ($\gamma_1 \neq 0, \gamma_2 = 0$), and the strongly decremental yaw strategies ($\gamma_1 - \gamma_2 > 20°$).

4. Conclusions

With the objectives of maximizing the power output and minimizing the fatigue loads, we perform a traversal search in a finite discrete decision space $\mathbf{\Gamma}$ spanned by the yaw angles of the first two turbines in a wind-turbine array subjected to AYC. The time series of the power output and the yaw moment are obtained from LES. The total mean power and the total DEL of the wind-turbine array are computed at every decision point in $\mathbf{\Gamma}$. By comparing the LES results and the wind-tunnel measurements for four representative yaw scenarios, we find that the predictions of the total mean power output obtained from LES are in good agreement with the experiment results, with the maximum relative error of 3.8%. As for the power predictions for each turbine, better consistency between LES and the experiments are found in the cases in

the cases with smaller wake superposition.

Inspecting the results of the power output and the yaw-moment DEL in the objective space $\mathbf{\Omega}$ spanned by these two metrics, we further find that applying a conservative yaw angle ($\gamma_1 < 10°$) for the first wind turbine is not efficient: it only achieves marginal power gains at the cost of significantly increasing the fatigue loads. Identifying the Pareto-optimal strategies in the decision space $\mathbf{\Gamma}$, we also find that the majority of the Pareto-optimal strategies belong to the category of moderately decremental yaw strategies, and they are clustered on a narrow band in the decision space. Such a result suggests that, with the load mitigation being taken into account, there exists a subspace in the decision space where the Pareto-optimal strategies are densely distributed. The search of the optimal AYC strategy can be largely confined within this subspace instead of the entire decision space. This property is particularly desirable for derivative-free optimization algorithms, such as genetic algorithms and simulated-annealing algorithms, which involve random sampling in the decision space.

In future studies, we plan to further investigate the distribution of Pareto-optimal strategies in high-dimensional decision spaces, corresponding to the cases with more turbines subjected to AYC. We are interested in examining whether a subspace clustered with Pareto-optimal strategies can still be found in higher dimensions. We also plan to study the application of AYC in a wind-turbine array consisting of real-scale turbines and evaluate if the Pareto-optimal strategies still mostly share the characteristic of moderately decremental yaw, as in the case of miniature wind turbines, and carry out similar analyses on the cases of partial wake overlapping.

Acknowledgements
This research was funded by the Swiss National Science Foundation (grant number: 200021_172538) and the Swiss Federal Office of Energy. In addition, this project was carried out within the frame of the Swiss Centre for Competence in Energy Research on the Future Swiss Electrical Infrastructure (SCCER-FURIES) with the financial support of the Swiss Innovation Agency (Innosuisse-SCCER programme, contract number: 1155002544). Computing resources were provided by EPFL through the use of the facilities of its Scientific IT and Application Support Center and by the Swiss National Supercomputing Centre (CSCS).

References

[1] Stevens R J A M and Meneveau C 2017 *Annu. Rev. Fluid Mech.* **174** 311-39.
[2] Porté-Agel F, Bastankhah M and Shamsoddin S *Bound-lay. Meteorol.* **49(1)** 1-59.
[3] Thomsen K and Sørensen P 1999 *J. Wind Eng. Ind. Aerod.* **80(1-2)** 121-36.
[4] Barthelmie R J, Frandsen S T, Nielsen M N, Pryor S C, Rethore E and Jørgensen H E 2007 *Wind Energy* **10(6)** 517-28.
[5] Wu Y T and Porté-Agel F 2015 *Renewable Energy* **75** 945–55.
[6] Meyers J and Meneveau C 2012 *Wind Enery* **15(2)** 305-17.
[7] Marden J R, Ruben S D and Pao L Y 2013 *IEEE T. Contr. Syst. T.* **21(4)** 1207-14.
[8] Dilip D and Porté-Agel F 2017 *Energies* **10(6)** 757.
[9] Fleming P A, Gebraad P M O, Lee S, Van Wingerden J W, Johnson K, Churchfield M, Michalakes J, Spalart P and Moriarty P 2014 *Renewable Energy* **70** 211-18.
[10] Howland M F, Lele S K and Dabiri J O 2019 *P. Natl. Acad. Sci.* **116(29)** 14495-500.
[11] Bastankhah M and Porté-Agel F 2019 *J. Renew. Sustain Ener.* **11(2)** 023301.
[12] Gebraad P M O, Teeuwisse F W, Van Wingerden J W, Fleming P A, Ruben S D, Marden J R and Pao L Y 2016 *Wind Energy* **19(1)** 95-114.
[13] Gebraad P M O, Thomas J J, Ning A, Fleming P and Dykes K 2017 *Wind Enery* **20(1)** 97-107.

[14] Archer C L and Vasel-Be-Hagh A 2019 *Sustain Energy Techn.* **33** 34-43.
[15] Munters W and Meyers J 2018 *Energies* **11(1)** 177.
[16] Kragh K A and Hansen M H 2014 *Wind Energy* **17(7)** 971-82.
[17] Jeong M S, Kim S W, Lee I, Yoo S J and Park K C 2013 *Renewable Energy* **60** 256-68.
[18] Van Dijk M T, Van Wingerden J W, Ashuri T and Li Y 2017 *Energy* **121** 561-69.
[19] Bartl J Mühle F and Sætran L 2018 *Wind Energy Sci.* **3** 489-502.
[20] Lau B C P, Ma E W M and Pecht M 2012 *P. IEEE 2012 Prog. Sys. Heal. Mana. Conf.* IEEE p 1-5.
[21] Porté-Agel F, Meneveau C and Parlange M B 2000 *J. Fluid Mech.* **415** 261-84.
[22] Stoll R and Porté-Agel F 2000 *Water Resour. Res.* **42** W01409.
[23] Wu Y T and Porté-Agel F 2011 *Bound-lay. Meteorol.* **138(3)** 345-66.
[24] Porté-Agel F, Wu Y T, Hao L and Conzemius R J 2011 *J. Wind Eng. Ind. Aerod.* **99(4)** 154-68.
[25] Lin M and Porté-Agel F 2019 *Energies* **12(23)** 4574.
[26] Bastankhah M and Porté-Agel F 2017 *Energies* **10(7)** 908.
[27] Freebury G and Musial W 2000 *2000 ASME Wind Energy Symp.* p 50.
[28] Blasque J and Natarajan A 2013 *Int. Conf. Comp. Meth. Mari. Eng.* p 818-29.
[29] Zalkind D S and Pao L 2016 *2016 Amer. Cont. Conf.* (IEEE) p 537-42.
[30] Fleming P, Annoni J, Churchfield M, Martinez-Tossas L A, Gruchalla K, Lawson M and Moriarty P 2018 *Wind Energy Sci.* **3(1)** 243-55.
[31] Martínez-Tossas L A, Annoni J, Fleming P A, and Churchfield M J 2019 *Wind Energy Sci.* **4** 127-38.
[32] Zong H and Porté-Agel F 2020 *J. Fluid Mech.* **A8** 890.